Supporting Information

Straume et al. 10.1073/pnas.1017909109

SI Results

Stable Down-Regulation of Heat Shock Protein 27 in an Angiogenic Human Breast Cancer Cell Line Induces Long-Term Dormancy in Vivo. Mice inoculated with heat shock protein (HSP) 27KD-2 cells had an approximate 1-wk delay in the onset of exponential tumor growth (starting on day 35). On day 77, HSP27 knockdown in HSP27KD-1 tumors resulted in 55% reduction in tumor volume (999 ± 624 mm^3; $n = 7$).

We performed a larger experiment comparing the negative nontargeted (NT) control and HSP27KD-3 cell lines (Fig. S1*A*). The control group ($n = 20$) and the HSP27KD-3 group ($n = 20$) differed significantly in the timing between tumor cell inoculation and the appearance of the first detectable tumor (i.e., size >~40 mm^3) ($P < 0.001$, log-rank test), as assessed by the Kaplan–Meier survival method. All mice injected with the control (high HSP27 expression) cell line initiated tumor growth at approximately 20 d after inoculation and had a mean tumor volume of 1,000 mm^3 by day 70. All but three mice inoculated with the HSP27KD-3 (low HSP27 expression) cell line had nonpalpable and microscopic tumors up to day 112 (Fig. S1*B*). Three of the HSP27KD-3 mice initiated tumor growth spontaneously and exhibited expanded tumor size, at days 70, 90, and 112.

Down-Regulation of HSP27 in an Angiogenic Human Breast Cancer Cell Line Results in Gene Expression Patterns Similar to Those Present in the Nonangiogenic Cell Line. We used gene set enrichment analysis (GSEA) (1) to identify gene signatures that were significantly enriched in MDA-MB-436-A nontargeted control cells relative to HSP27 knockdown cells. Ablation of HSP27 expression resulted in a significant shift away from angiogenesis-related expression signatures, such as hypoxia, VEGF-A, HIF1 targets, and STAT3 targets (Table S2 and Fig. S5 *A* and *B*). In addition, NFκB and STAT3 activation signatures were significantly associated with HSP27 expression and KEGG pathways related to ECM receptor interaction, focal adhesion, and VEGF-A signaling pathways (Table S2). Collectively, our findings indicate that HSP27 expression is functionally linked to elevated expression of genes related to angiogenic pathways, as well as activation of STAT3 and NFκB transcription factors.

Suppression of HSP27 Leads to Reduced VEGF-A, VEGF-C, and Basic Fibroblast Growth Factor. Control cells contained 2.1-fold higher levels of VEGF-A mRNA compared with HSP27KD-3 cells, as assessed by real-time quantitative PCR (control NT, 1 vs. HSP27KD-3, mean 0.47 ± 0.039; $P < 0.001$, *t* test) (Fig. 3*C*), indicating that HSP27 regulates VEGF-A expression at the transcriptional level. Expression of the angiogenic ligands VEGF-C, angiopoietin-1, angiopoietin-2, placental growth factor, and platelet-derived growth factor were compared in control NT and HSP27KD-3 cell pellets created in in vitro experiments and stained by immunohistochemistry, but no statistically significant differences were detected. In the in vivo experiments, VEGF-C protein staining showed a tendency toward greater strength of control NT tumors compared with HSP27KD-3 tumors [staining index (SI), 1.8 ± 0.4 vs. 0.4 ± 0.4; $P = 0.06$, χ^2 test) (Fig. S4).

Dual immunohistochemical staining of HSP27 protein and VEGF-A proteins was performed on angiogenic (MDA-MB-436-A) and nonangiogenic (MDA-MB-436-NA) cell pellets and in vivo tumors, as well as on experimental HSP27KD-3 and NT tumors. In general, a mixed expression pattern was observed, with some cells appearing positive for VEGF-A only, others appearing positive for HSP27, and still others with coexpression of the two (Fig. S4).

Hypoxic conditions (1% O_2 overnight) resulted in 2.2-fold increase in VEGF-A secretion from both control cells (mean normoxic, 690 ± 52.8 pg/mL vs. mean hypoxic, 1,492.7 ± 276.6 pg/mL; $P = 0.046$, *t* test) and HSP27KD-3 cells (mean normoxic, 253.0 ± 25.9 pg/mL vs. mean hypoxic, 498.2 ± 44.0 pg/mL; $P = 0.009$, *t* test) (Fig. 3*G*). Hypoxic conditions induced significantly increased secretion of basic fibroblast growth factor (bFGF) from the control cells (mean normoxic, 46.4 ± 2.0 pg/mL vs. mean hypoxic, 136.8 ± 15.5 pg/mL; $P = 0.002$, *t* test), but not from HSP27KD-3 (mean normoxic, 8.3 ± 0.9 pg/mL vs. mean hypoxic, 7.0 ± 2.7 pg/mL; $P = 0.4$, *t* test) (Fig. 3*H*). As quantified by ELISA, hypoxia induced a 8.8-fold increase in HSP27 phosphorylation within the control cell line (mean normoxic, 42.1 ng/mL ± 16.3 ng/mL vs. mean hypoxic, 369.8 ± 61.3 ng/mL; $P = 0.007$, *t* test), but had no apparent effect on the HSP27KD-3 cell line (mean normoxic, 20.3 ± 3.9 ng/mL vs. mean hypoxic, 10.0 ± 2.1 ng/mL; $P = 0.08$, *t* test).

HSP27KD-3 cells secreted 1.7-fold lower levels of bFGF compared with control NT cells, but contained 2.3-fold higher intracellular bFGF (Fig. 3 *E* and *F*). These findings suggest an impaired mechanism of bFGF transport across the cell membrane when HSP27 is low or absent. In contrast to HSP27KD-3 cells, HSP27 protein more frequently colocalized with bFGF within control NT cells under normoxic conditions (Fig. S4 *D–I*), as assessed by confocal microscopy.

Suppression of HSP27 Does Not Significantly Alter Tumor Cell Proliferation, G1-S Cell Cycle Progression Markers, or Apoptosis. The effect of HSP27 knockdown on tumor cell proliferation and apoptosis was assessed by comparing in vitro growth kinetics in the control cells (with high HSP27 expression) and the HSP27KD-3 cell line (with low HSP27 expression). No significant difference in the in vitro growth curves was seen between the control cells and HSP27KD-3 cells (Fig. 4*E*). Tumor samples from in vivo experiments exhibited no statistically significant difference in the proliferation of HSP27KD-3 tumor cells versus control NT cells (Fig. 4 *G–I*). Nonetheless, in dormant tumors (HSP27KD-3), tumor cells ($n = 8$) proliferated at lower rate than the control tumors ($n = 18$) (mean rate, 70.6% ± 11.3% vs. 81.2% ± 2.3%; $P = 0.11$, *t* test) (Fig. 4 *G–I*). Consistent with previous observations on cellular proliferation, no differences in cyclin A or cyclin D1 protein expression were detected (Fig. S4). In addition, a borderline significant increase in apoptotic rate was detected by TUNEL staining in the HSP27KD-3 tumors ($n = 7$) compared with control NT tumors ($n = 17$) (6.7% ± 1.7% vs. 4.5% ± 0.4%; $P = 0.09$, *t* test) (Fig. 4 *J–L*). These data suggest that down-regulation of HSP27 inhibits primarily the angiogenic switch in our model, and that this effect linked to tumor dormancy and growth inhibition.

One of the animals carrying a dormant microscopic HSP27KD-3 tumor was killed on day 56 after inoculation, after which a tumor piece was isolated and allowed to grow in culture (Fig. S3*A* and *B*). Under in vitro conditions, tumor cells actively migrated from the tumor piece onto the plastic and began to proliferate (Fig. S3*B*). The in vitro growth curve of the resulting new cell line (Fig. S3*C*) demonstrates that these cells were able to proliferate similarly to the original control and HSP27KD-3 cells shown in Fig. 4*E*.

To examine a possible G1-S cell cycle block, we performed immunohistochemical staining of two regulators of the G1-S cell cycle checkpoint, cyclin D1 and cyclin A. Neither HSP27KD-3 cells nor NT cells expressed cyclin D1 in the presence of internal positive controls (Fig. S4). The mean cyclin A SI was 6.2 ± 1.0 in

HSP27KD-3 cells, compared with 5.9 ± 0.6 in the NT cells (Fig. S4). The in vitro experiments revealed no significant difference between the cell lines in terms of cyclin D1 expression (NT mean, 1.3 ± 0.3; HSP27KD-3 mean, 1.0 ± 0.1) or cyclin A (NT mean, 8.0 ± 1.0; HSP27KD-3 mean, 5.0 ± 2.1).

Stable Up-Regulation of HSP27 in Nonangiogenic Human Breast Cancer Cells Induces Expansive Tumor Growth in Vivo. Supporting our hypothesis, HSP27 tagged with GFP (HSP27-GFP) was overexpressed in the nonangiogenic MDA-MB-436NA (with intrinsically low HSP27; Fig. 1*A*) cells (Fig. 2*E*). A weak endogenous HSP27 band was observed in the control cells infected with pCMV6-neo vector, likely due to the stress introduced by the procedure (Fig. 2*E*). In the HSP27OE cells, HSP27-GFP overexpression also resulted in an increase of HSP27 in addition to the HSP27-GFP band (Fig. 2*E*). SCID mice ($n = 5$ per group) were inoculated s.c. with HSP27-overexpressing (HSP27OE) cells and compared with the negative vector control cells and the parental nonangiogenic cells. HSP27OE cells initiated exponential tumor growth at day 40 and reached a mean size of 1586 mm^3 by day 70 (Fig. 2*G*). In comparison, mice inoculated with parental cells formed microscopic, nonpalpable tumors (<40 mm^3) and persisted up to day 70 without switching to the angiogenic phenotype, whereas the control vector cells reached a mean size of 209 mm^3 by day 70. HSP27 protein staining by immunohistochemistry was significantly stronger in the HSP27OE tumors compared with control vector tumors (mean SI, 5.0 vs. 2.4; $P = 0.006$, χ^2 test). In addition, the mean vascular proliferation index was significantly higher in the HSP27OE tumors compared with control tumors (mean, 18.5% vs. 9.0%; $P = 0.001$, t test).

SI Materials and Methods

In Vitro Cell Culture. The establishment of a nonangiogenic (MDA-MB-436 A1) and an angiogenic (MDA-MB-436 A) breast cancer cell line has been described in detail previously (2). In brief, cell lines were defined as nonangiogenic based on (*i*) the absence of angiogenic activity, as evidenced by repulsion of existing blood vessels and/or absence of microvessels within the tumor; (*ii*) their growth to only ≤~1 mm in diameter in vivo, at which time further expansion stopped; (*iii*) the apparent absence of "tumor take" for at least 130–238 d, until the emergence of the angiogenic phenotype; and (*iv*) the fact that the tumors remained harmless to the host until they switched to the angiogenic phenotype. Furthermore, the angiogenic cell lines expressed increased VEGF-A and bFGF and decreased TSP-1, and induced increased MVD and vascular permeability when grown in mice. All cell lines were maintained under standard tissue culture conditions (37 °C, 5% CO_2, humidified atmosphere). The unmodified human breast cancer (MDA-MB-436) cells were grown in DMEM (Invitrogen) with 10% (vol/vol) FBS. The modified cell clones with HSP27 knockdown were maintained in RPMI 1640 (Invitrogen/Gibco) with 10% FBS and 2 μg/mL of puromycin (InvivoGen) 5 μg/mL. The modified cell clones overexpressing GFP-tagged HSP27 were maintained in RPMI 1640 with 10% FBS supplemented with 1,000 μg/mL of G418 (Invitrogen/Gibco).

In vitro growth curves were generated by plating 5×10^4 cells in 35-mm dishes in triplicate. Cells were counted daily over a 13-d period. Cell pellets were made by centrifuging cells scraped from four confluent 150-mm dishes and fixed in formalin. The in vitro hypoxic stress experiments were performed in a Ruskinn inVivo2 model 400 hypoxia workstation at 37 °C in 1% O_2, 7% CO_2, and 92% N_2. When the cells reached confluence or subconfluence (~60–70%), depending on the experiment, cells were incubated in the hypoxia work chamber overnight on 15-cm plates and then compared with cells incubated under normal cell culture conditions. Care was taken to fix the cells in 4% formalin promptly after they were removed from the hypoxic chamber, to avoid exposure to normoxic air that might affect phosphorylation of HSP27. Sampling for analyses in supernatant or cell lysates also was performed promptly (within 60 s) after the plates were removed from the hypoxic chamber.

Knockdown of HSP27 Protein Expression, shRNA Constructs, Lentiviral Infection, and siRNA Transfection. shRNA constructs were cloned in a pLKO 1 puromycin vector designed by the Harvard/MIT RNAi consortium and distributed by Open Biosystems. Sequences were as follows: NT: 5′-CAACAAGATGAAGAGCACCAA-3′; TRCN0000008752: 5′-CCCAAGTTTCCTCCTCCCTGT-3′; TRCN0000008753: 5′-CCGATGAGACTGCCGCCAAGT-3′; TRCN0000008754: 5′-GATCACCATCCCAGTCACCTT-3′. Lentiviral production and infection were performed as described previously (3). After puromycin selection, cells stably knocking down HSP27 were identified by Western blot analysis.

Lentiviruses carrying NT shRNA sequences were used as a control. In addition to the NT control cell line, three separate HSP27 knockdown cell lines were established using three different shRNA sequences against HSP27, designated HSP27KD-1, HSP27KD-2, and HSP27KD-3. HSP27 expression levels were quantified by Western blot analysis using the NT control and three HSP27 knockdown cell lines (Fig. 2*A*).

Establishment of MDA-MB436NA Cells Overexpressing HSP27. pCMV6-HSP27-GFP-neo constructs were obtained from Origene. Once incorporated in the mammalian cells and after selection with neomycin (G418), this vector stably expresses HSP27 protein tagged with GFP. The accession number for the HSP27 cDNA is NM_001540.2. Exponentially growing MDA-MB436NA cells with low HSP27 protein expression confirmed by Western blot analysis were used. In brief, 1×10^6 cells were transfected with either 10 μg of pCMV6-HSP27-GFP-neo or 10 μg of pCMV6-neo vectors using Fugene HD (Roche) following the manufacturer's instructions. At 24 h posttransfection, the transfected cells were subject to antibiotic selection at 1,000 μg/mL of G418. Cytostatic effects were observed initially, and cell lines constitutively overexpressing HSP27-GFP were established after G418 selection for 14 d. Overexpression of HSP27 was confirmed by Western blot analysis using HSP27 antibody (Fig. 2*E*).

Microarray Analysis. The Agilent Human Whole Genome (4 × 44k) Oligo Microarray with Sure Print Technology was used for microarray analysis. Total RNA was extracted from subconfluent monolayers of cells using the E.Z.N.A RNA Purification Kit (Omega Bio-Tek) and stored at −80 °C. Quality and yield of total RNA were assessed with an Agilent 2100 Bioanalyzer and ethidium bromide-stained 1% agarose gel electrophoresis and PowerWave spectrophotometry (Omega BioTek) at absorption wavelengths of 260 nm and 280 nm. Then 1 μg of DNase-treated total RNA was converted into cDNA and Cy3-labeled cRNA using the Agilent Low RNA Input Linear Amplification Kit PLUS One-Color Kit in accordance with the manufacturer's instructions. Hybridization of Cy3-labeled cRNA targets to the oligonucleotide microarrays (Agilent Cat. no. G4112F, 4x44k) followed the instructions of the manufacturer (Agilent Cat. no. 5188-5242), and washed microarrays were scanned (Agilent Scanner G2505B) and fluorescent Cy3 hybridization signals were automatically extracted using the Agilent Feature Extraction v.7.5. software as described previously (4). After cleanup of labeling reactions using the Qiagen RNAeasy Mini Kit, incorporation of Cy3 into cRNA was measured by absorption readings at 550 nm, using a PowerWave spectrophotometer (Omega BioTek). Parallel readings at 260 nm allowed calculation of specific Cy3 labeling of cRNA targets. Hybridization and further processing of DNA microarray data have been described previously (4).

After normalization, ANOVA and significant analysis of microarrays of the J-Express program package (www.molmine.com) (5) were used to identify differentially expressed genes.

The samples were divided into two groups, and gene expression levels were compared between the angiogenic (MDA-MB-436 A) and nonangiogenic (MDA-MB-436 A1) cell lines and between HSP27KD-3 cells and NT control cells.

GSEA (www.broad.mit.edu/gsea) (1) was performed across the complete list of genes ranked by the *t* test. Gene sets associated with KEGG pathways, as well as hypoxia, angiogenesis, and NFκB and STAT3 activation used in the GSEA analysis, were obtained from the Molecular Signatures Database (www.broad.mit.edu/gsea/msigdb).

When relating HSP27 expression with survival in human breast cancer patients, genes down-regulated by HSP27 knockdown in angiogenic MDA-MB-436A cells with a fold change >2 and a false discovery rate (FDR) P value < 0.05 were considered components of a HSP27 gene expression signature. HSP27 signature genes were matched to the corresponding gene symbols in three different breast cancer datasets (downloaded from jura.wi.mit.edu/bioc/benporath) (6). Datasets were first log2-transformed, mean-centered, and loaded into Genomica software (www.genomica.weizmann.ac.il). Each patient was assigned an enrichment score using a hypergeometric test and a, FDR calculation to account for multiple hypothesis testing ($P < 0.05$; FDR <0.05). For each dataset, two main clusters were classified by positive or negative enrichment of HSP27 signature and were matched with survival data. Classification by HSP27 expression status was also related to the molecular subtype of breast cancer. Statistical significance was calculated by the log-rank test, and Kaplan–Meier plots were created with GraphPad software.

Western Blot Analysis. Protein concentrations were determined by the BioRad protein assay. For this assay, 60 μg of protein per well were loaded onto a 4–12% precast Bis-Tris gel (BioRad). The protein extracts were electrophoresed and transferred to an Immobilon-P membrane (Millipore). The membranes were blocked in 5% nonfat milk and incubated with primary antibodies to Tsp-1 (Ab-11; LabVision), c-Myc (Santa Cruz Biotechnology), and β-actin (AbCam). The membranes were then washed in PBS plus 0.1% Tween-20 and incubated with either HRP-conjugated goat anti-mouse or anti-rabbit secondary antibody (Jackson ImmunoResearch), followed by another washing. The membrane was then developed with ECL reagent (Pierce) and exposed on film.

ELISA Quantification of VEGF-A, VEGF-C, bFGF, Total HSP27, and Phospho-HSP27. The control NT and HSP27KD-3 cells were plated in triplicate and incubated until confluence. At confluence, the medium was replaced with serum-free medium (1% FCS for the VEGF-A and VEGF-C analyses) and serum-starved overnight. The medium was then collected, and ELISA kits were used to determine concentrations of human VEGF-A and VEGF-C (R&D Systems), human bFGF (R&D Systems), total HSP27 (Assay Designs), and phospho-HSP27 (Biosource/Invitrogen), in accordance with the manufacturer's protocols. To collect cell lysates for analyses of intracellular concentration of the same proteins as above in addition to TSP-1 and c-Myc, cells were lysed in mammalian protein extraction reagent (M-PER; Pierce) in accordance with the manufacturer's protocol, after removal of media and PBS wash. Cell lysates were scraped from the plate and briefly centrifuged, and supernatant was used for further analyses (ELISA and Western blot). For each sample, blank samples (i.e., serum-free media or cell lysate buffer) were subtracted, and mean results were normalized for 1×10^6 cells. These assays were done in triplicate.

Real-Time Quantitative PCR. Total cellular RNA was extracted from NT control cells and HSP27KD-3 cells using the E.Z.N.A Total RNA Kit (Omega Bio-Tek). cDNA was synthesized using 500 ng of the RNA template with SuperScript III First-Strand Synthesis SuperMix (Invitrogen) for quantitative RT-PCR (qRT-PCR). VEGF-A expression was evaluated by real-time qRT-PCR using the DNA Engine Opticon 2 Continuous Fluorescence Detection System (BioRad). For detection of VEGF-A, the forward primer 5′-AGACCCTGGTGGACATCTTCC-3′ and reverse primer 5′-TGATCCGCATAAT-CTGCATGG-3′ were used in combination with 1 μL of cDNA and SYBR GreenER qPCR Supermix (Invitrogen). The qRT-PCR results were normalized by the expression levels of GAPDH. Relative gene expression was calculated using the $2^{-\Delta\Delta C}{}_T$ method (7).

Subcutaneous Tumor Growth. SCID male mice aged 6–8 wk (obtained from Massachusetts General Hospital, Boston, MA) were used for in vivo studies and cared for in accordance with the standards of the Institutional Animal Care and Use Committee under a protocol approved by the Animal Care and Use Committee of Children's Hospital Boston. To begin, 1×10^6 cells in 0.2 mL of PBS were inoculated s.c. in the lower right quadrant of the flank for all cell lines tested. Once tumors became palpable (~40 mm^3), tumor size was measured once a week. Mice were killed by cervical dislocation when tumors reached ~1,500 mm^3 in diameter. Representative mice were killed by cervical dislocation at various time points for microscopic examination.

Tissue Handling and Immunohistochemistry. Cell pellets were prepared from cells grown in culture by centrifuging cells ($350 \times g$, 5′) scraped from four confluent 150-mm dishes and fixed in formalin. Cell pellets, as well as tumor samples from the animal experiments, were fixed in 4% formalin overnight and then embedded in paraffin as described previously (2). Tissue microarray blocks of patient samples were prepared as reported in detail previously (8, 9). Immunohistochemical analysis was performed on formalin-fixed and paraffin-embedded tissue or tumor cell pellets from tissue culture. After deparaffinization and rehydration through xylene and alcohols, antigen retrieval was performed by treatment in a pressure cooker for 30 s at 125 °C in Target Retrieval Solution (Dako). Then 4-μm-thick sections were incubated for 30 min with polyclonal goat anti HSP27 (sc-1048, 1:100 dilution; Santa Cruz Biotechnology). Specific staining signals were detected by a goat ABC staining system (sc-2023; Santa Cruz Biotechnology). Serial sections incubated with primary antibody and 10-fold excess of blocking peptide (sc-2023 P) served as negative control. For STAT3, sections were incubated with monoclonal rabbit anti-human phospho-STAT3 (ser727), phospho-STAT3 (tyr705), and total-STAT3 (all from Cell Signaling) at 1:50 overnight, 1:25 overnight, and for 60 min at room temperature, respectively. Similarly, sections were incubated overnight with VEGF-C (ab9546), platelet-derived growth factor (ab9704), placental growth factor (ab9542), angiopoietin-1 (ab8451), angiopoietin 2 (ab65835), cyclin D1 (ab16633), and cyclin A (ab7956), diluted 1:100. Specific staining signals were detected by the EnVision Staining System (K-4009; Dako). For NFκB, sections were incubated for 30 min with polyclonal rabbit anti-NFκB (sc-109, 1:100 dilution; Santa Cruz Biotechnology). Specific staining signals were detected by rabbit on rodent polymer (Biocare), with a blocking peptide (sc-109 P) as a negative control. For microvascular proliferation, a sequential staining method was applied for the double staining of rat anti-CD34 (ab8158; Abcam) and rat anti-Ki-67 (M7249; Dako). This Ki-67 antibody is particularly useful for analysis of human tumor growth in mouse tissue, because it is mouse-specific and does not stain proliferating human tumor cells. Ki-67 was detected by alkaline phosphatase-conjugated goat anti-rat secondary antibody (sc-3824) and stained by fast blue. Subsequently, remaining rat antibody in the tissue was denatured using a denaturing solution kit (DNS001H; Biocare Medical) for 3 min, after which sections were incubated with anti-CD34, which was detected by HRP-conjugated secondary antibody (sc-3823) and stained with 3-amino-9-ethylcarbazole (red). Ki-67 staining

and CD34 single staining were performed at the Dana-Farber Harvard Cancer Center core facility or The Gade Institute core facility in accordance with standard protocols. TUNEL staining was performed using the TACS2 TdT-DAB In Situ Apoptosis Detection Kit (Trevigen).

The HSP27 knockdown cell line HSP27KD-3 and NT control cells were cultured on coverslips coated with 1% gelatin. At 60–80% confluence, cells were fixed in 4% formalin and permeabilized with 0.5% Triton. Cells were then incubated with anti-bFGF (sc-79; Santa Cruz Biotechnology), anti-HSP27 (sc-1048; Santa Cruz Biotechnology), or anti-phospho (ser 82) HSP27 (44-5346; Biosource) incubated at 1:100 dilution for 60 min at room temperature in double-staining experiments. Goat antibody signals were detected by FITC-conjugated donkey anti-goat secondary antibody (sc-2024; Santa Cruz Biotechnology), and rabbit antibodies were detected by biotinylated donkey anti-rabbit antibody (sc-2089; Santa Cruz Biotechnology), both incubated simultaneously for 30 min and diluted 1:250. Biotin was detected by streptavidin-conjugated Texas Red. DAPI was used for nuclear counterstaining.

Evaluation of Staining Results. An SI, obtained as a product of staining intensity (0–3) and proportion of immunopositive tumor cells (<10%, 1; 10–50%, 2; >50%, 3) was calculated as described previously for HSP27, STAT3, and NFκB staining (10).

Microvessel density (MVD) was assessed following the method of Weidner et al. (11) and expressed as number of microvessels per square millimeter. In brief, "hot spot" areas were identified at low magnification. Within these areas, a maximum of 10 consecutive high-power fields (HPFs) were counted on 400× magnification. Any highlighted endothelial cell or cell cluster that was clearly separate from adjacent microvessels was counted (12). The ratio of the number of tumor-associated vessels with Ki-67-positive endothelial nuclei (proliferating MVD) to the total number of vessels (MVD) was calculated (13).

Endothelial Cell Migration Assay. Human umbilical vein endothelial cells (HUVECs; Lonza) were maintained according to the manufacturer's directions. Low-passage (no more than passage seven) cells were grown to subconfluence and used for the migration experiments. Endothelial cell migration assays were performed in a modified Boyden chamber (6.5-mm diameter, 10-μm thick, 8-μm pores; Costar Transwell; Corning) coated with 10 μg/mL of fibronectin in PBS overnight at 4 °C. EBM basal medium (Lonza) supplemented with 0.5% BSA and plates with 50,000 cells per well in the upper chamber were used. HUVECs were allowed to migrate for 4 h. Adherent cells were fixed and stained using the Hema-3 Manual Staining System (Fisher Diagnostics) following the manufacturer's instructions. Nonmigratory cells were removed with a cotton swab, and the number of migratory HUVECs per membrane was quantified using a 10× objective. Each sample was plated in triplicate. The average of three individual wells is given, with error bars representing SE. Each experiment was repeated twice.

Patient Series and Clinical Samples. The patient material in these series has been described in detail elsewhere (8, 14). In brief, the breast cancer samples were included from a nested case-control study as part of the Norwegian Breast Cancer Screening Program (15). Between 1996 and 2001, a total of 95 invasive interval cancers were recorded in Hordaland County, Norway. These cases were size-matched with 95 screen-detected cancers. Tissue collected from these cancers was mounted in tissue microarray blocks. Sufficient tumor tissue was available for 74 interval cancers and 59 screen-detected cancers. All vertical growth-phase melanomas recorded in Hordaland County between 1981 and 1997 were included as well (14). Complete information on patient survival and time and cause of death was available in all cases. Tissue from archival material of primary tumors was mounted in triplicate in tissue microarray blocks. Sufficient tumor tissue for evaluation of HSP27 staining was available in 97 cases.

Statistics. Statistical analyses were performed using SPSS 15.0 (IBM) and SigmaStat 3.0 (Systat). Differences between categorical variables were assessed using Pearson's χ^2 test. Continuous variables were compared between groups using the *t* test or the Mann–Whitney *U* test, depending on distribution. Univariate survival analyses were performed using the Kaplan–Meier method, and differences were evaluated by the log-rank test. Multivariate survival analyses were analyzed by the Cox proportional hazards method with the likelihood ratio test. Model assumptions were tested by log-log plots, and significant variables were tested for interactions.

1. Subramanian A, et al. (2005) Gene set enrichment analysis: A knowledge-based approach for interpreting genome-wide expression profiles. *Proc Natl Acad Sci USA* 102:15545–15550.
2. Naumov GN, et al. (2006) A model of human tumor dormancy: An angiogenic switch from the nonangiogenic phenotype. *J Natl Cancer Inst* 98:316–325.
3. Shimamura T, et al. (2008) Hsp90 inhibition suppresses mutant EGFR-T790M signaling and overcomes kinase inhibitor resistance. *Cancer Res* 68:5827–5838.
4. Ke XS, et al. (2009) Genome-wide profiling of histone h3 lysine 4 and lysine 27 trimethylation reveals an epigenetic signature in prostate carcinogenesis. *PLoS ONE* 4:e4687.
5. Dysvik B, Jonassen I (2001) J-Express: Exploring gene expression data using Java. *Bioinformatics* 17:369–370.
6. Ben-Porath I, et al. (2008) An embryonic stem cell-like gene expression signature in poorly differentiated aggressive human tumors. *Nat Genet* 40:499–507.
7. Livak KJ, Schmittgen TD (2001) Analysis of relative gene expression data using real-time quantitative PCR and the $2^{-\Delta\Delta CT}$ method. *Methods* 25:402–408.
8. Collett K, et al. (2005) A basal epithelial phenotype is more frequent in interval breast cancers compared with screen-detected tumors. *Cancer Epidemiol Biomarkers Prev* 14:1108–1112.
9. Straume O, Akslen LA (2002) Importance of vascular phenotype by basic fibroblast growth factor, and influence of the angiogenic factors basic fibroblast growth factor/fibroblast growth factor receptor-1 and ephrin-A1/EphA2 on melanoma progression. *Am J Pathol* 160:1009–1019.
10. Straume O, Akslen LA (2001) Expresson of vascular endothelial growth factor, its receptors (FLT-1, KDR), and TSP-1 related to microvessel density and patient outcome in vertical growth phase melanomas. *Am J Pathol* 159:223–235.
11. Weidner N, Semple JP, Welch WR, Folkman J (1991) Tumor angiogenesis and metastasis—correlation in invasive breast carcinoma. *N Engl J Med* 324:1–8.
12. Straume O, Salvesen HB, Akslen LA (1999) Angiogenesis is prognostically important in vertical growth phase melanomas. *Int J Oncol* 15:595–599.
13. Arnes J, Stefansson I, Brunet J, Foulkes W, Akslen L (2007) Vascular proliferation is a strong and independent prognostic factor in breast cancer. *Virchows Arch* 451:137.
14. Straume O, Sviland L, Akslen LA (2000) Loss of nuclear p16 protein expression correlates with increased tumor cell proliferation (Ki-67) and poor prognosis in patients with vertical growth phase melanoma. *Clin Cancer Res* 6:1845–1853.
15. Wang H, et al. (2001) Interval cancers in the Norwegian breast cancer screening program: Frequency, characteristics and use of HRT. *Int J Cancer* 94:594–598.

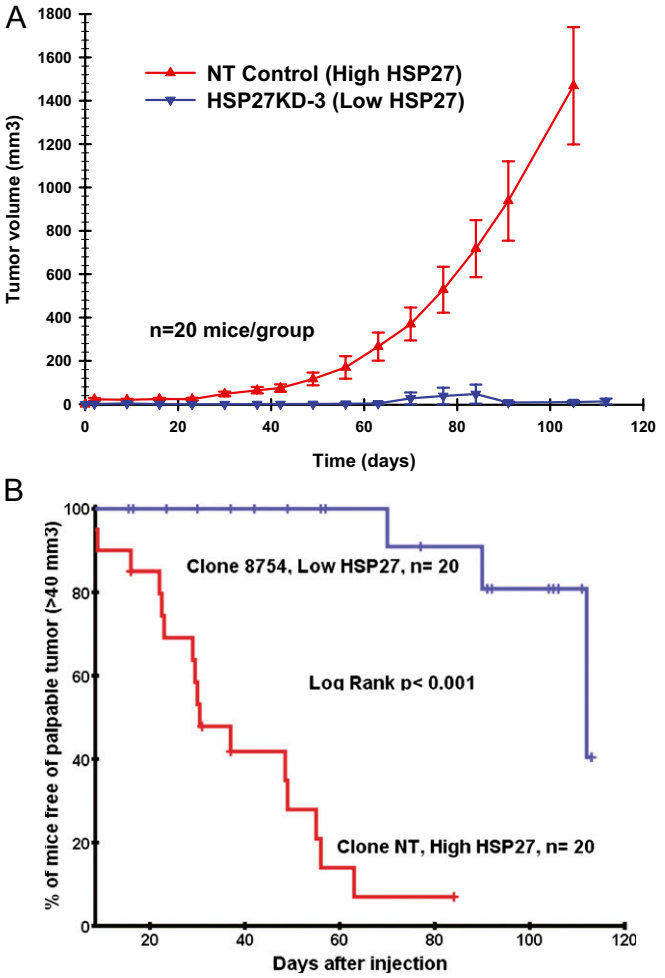

Fig. S1. (*A*) A separate xenograft experiment with 20 NT control mice and 20 HSP27KD-3 mice was performed to confirm and reproduce the results shown in Fig. 2. (*B*) The same dataset as in *A* was analyzed by a Kaplan–Meier plot of the time to a palpable tumor. A drop in the curve indicates the occurrence of a palpable tumor (>40 mm^3) at the corresponding time since cancer cell inoculation, and tick marks indicate euthanization for histological analysis of mice without palpable tumors (i.e., censored data). The difference in time to a palpable tumor was evaluated using the log-rank test.

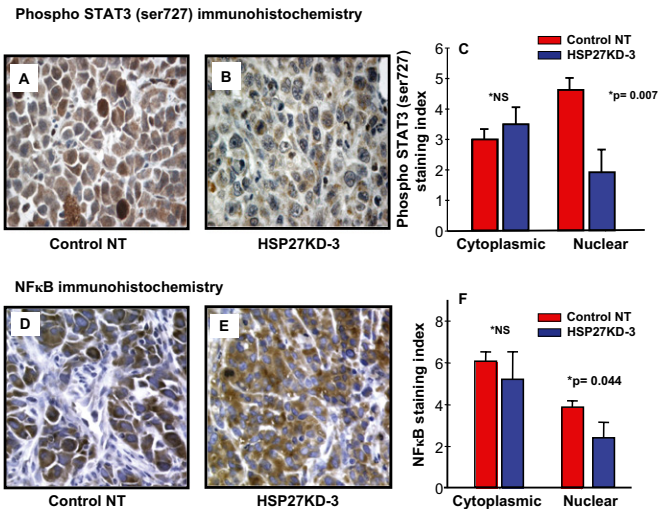

Fig. S2. High expression of HSP27 is associated with increased nuclear expression of transcription factors. (*A* and *B*) Phospho-STAT3 (ser 727) and NFκB staining by immunohistochemistry. The nuclear SI index was significantly higher in control NT tumors (*A*) compared with HSP27KD-3 tumors (*B*). (*C*) In contrast to nuclear staining, the cytoplasmic SI did not differ significantly between the tumor types. (*D–F*) In contrast to cytoplasmic staining, nuclear NFκB expression was significantly increased in control NT cells (*D*) compared with HSP27-KD3 cells (*E* and *F*).

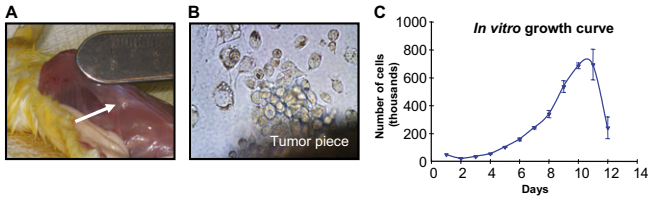

Fig. S3. (*A*) To demonstrate maintained proliferative capacity, a mouse carrying a dormant microscopic tumor from the HSP27KD-3 cell line was killed at day 56 after inoculation, and a tumor piece was isolated and allowed to grow in culture. (*B*) Under in vitro conditions, tumor cells actively migrated from the tumor piece onto the plastic and began to proliferate. (*C*) The in vitro growth curve of the resulting cell line shows that these cells were able to proliferate similarly to the original control and HSP27KD-3 cells shown in Fig. 4*E*.

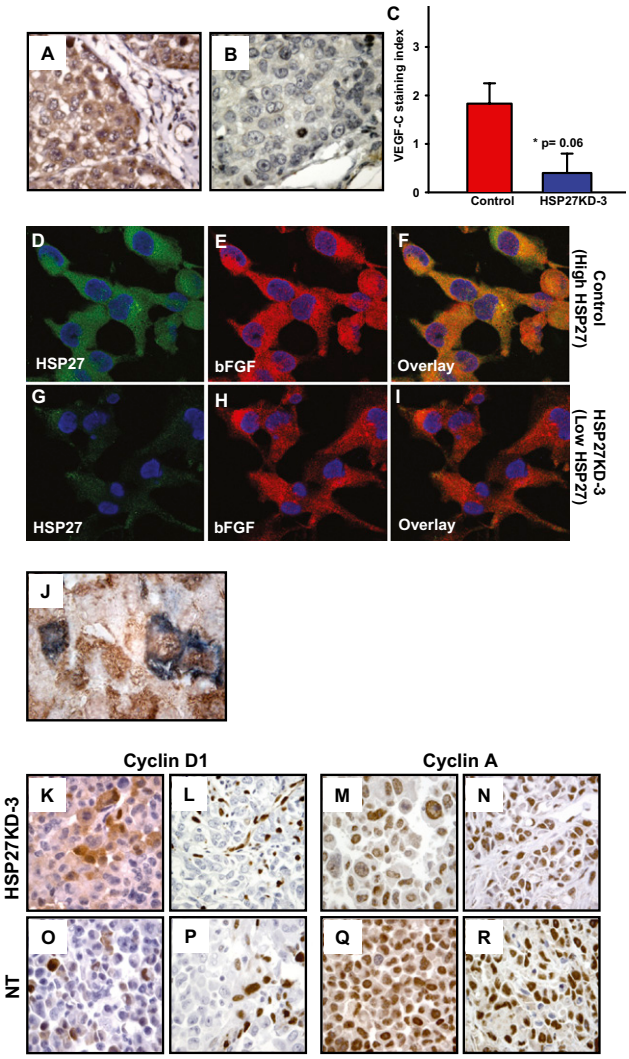

Fig. S4. (*A*–*C*) By immunohistochemistry, VEGF-C protein staining was stronger in the control NT tumors (*A*) than in HSP27KD-3 tumors (*B*), although the difference was not statistically significant (*C*). (Original magnification 400×.) (*D*–*I*) By immunofluorescence double-staining for HSP27 and bFGF in cells, co-localization of HSP27 protein and bFGF was observed more frequently in the control cells compared with HSP27KD-3 cells. (Original magnification, 1,000×). (*J*) Dual immunohistochemical staining of HSP27 protein (blue) and VEGF-A (brown) was performed on angiogenic (MDA-MB-436-A) and nonangiogenic (MDA-MB-436-NA) cells. (Original magnification, 1,000×). (*K*–*R*) There was no significant difference in the immunohistochemical expression of cyclin D1 (*K*, *L*, *O*, and *P*) or cyclin A (*M*, *N*, *Q*, and *R*) between HSP27KD-3 (in vitro pellet, *K* and *M*; in vivo tumor, *L* and *N*) and NT (in vitro pellet, *O* and *Q*; in vivo tumor, *P* and *R*).

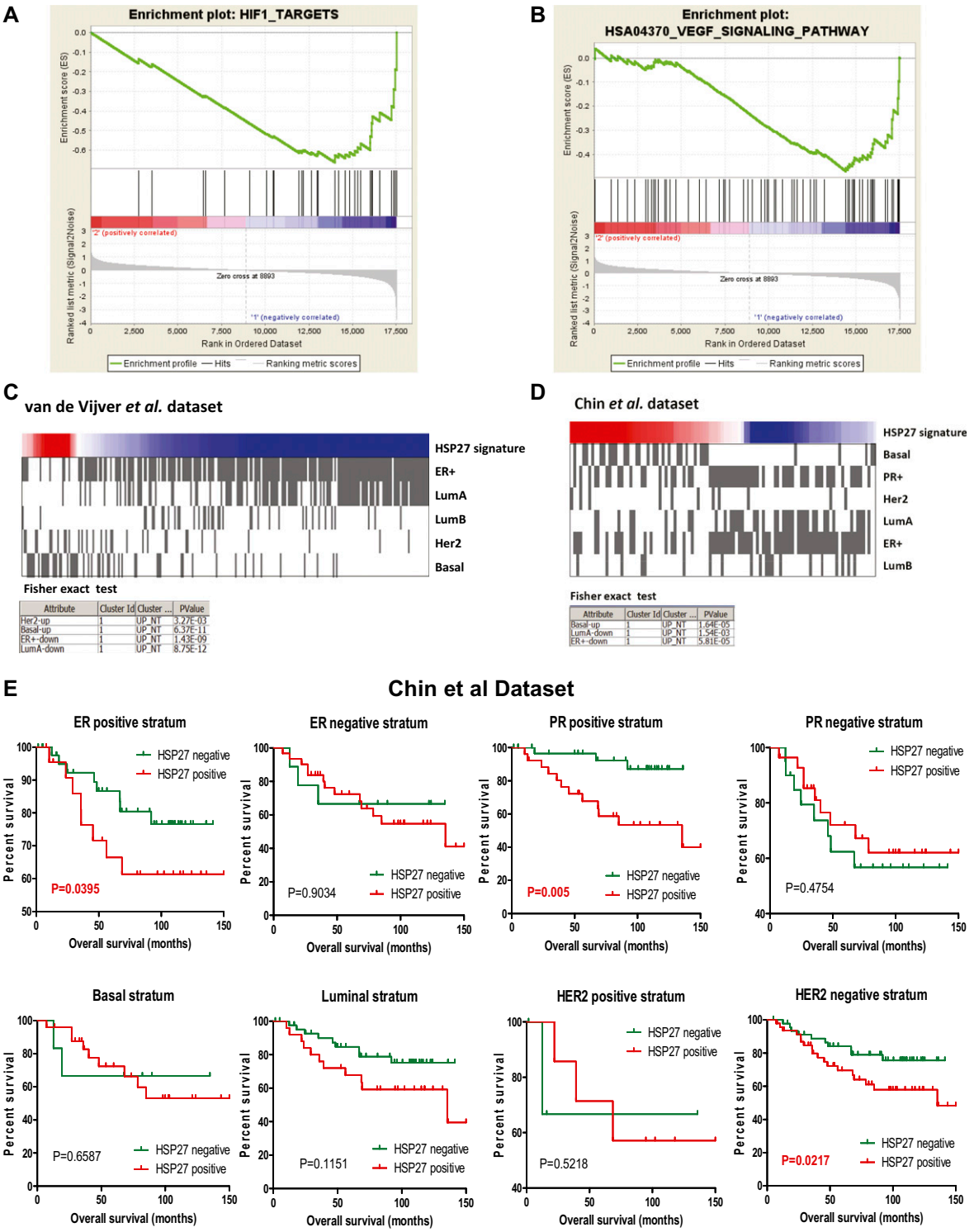

Fig. S5. Representative GSEA plots highlighting down-regulation of HIF1 (*A*) and VEGF-A (*B*) signatures in human breast cancer cells after HSP27 knockdown. Plots represent the enrichment score (ES), an estimation of the degree to which genes belonging to a given signature are overrepresented at the top (*Left*; HSP27KD) or bottom (*Right*; nontargeted control) of a ranked list of genes. The position of individual genes of the signature in the ranked list is indicated by vertical lines. (*C* and *D*) Associations between the HSP27 expression signature status (red, positive; blue, negative) and molecular subgroups and phenotypes of breast cancer, the van de Vijver dataset (*C*) and the Chin dataset (*D*). (*E*) Survival analysis (Kaplan–Meier plots, log-rank test) of breast cancer cases (Chin dataset) according to molecular subgroups and phenotypes. HSP27 expression signature-positive cases are shown in red.

Table S1. Significantly up-regulated or down-regulated genes by gene expression analysis in angiogenic versus nonangiogenic breast cancer cells as well as in angiogenic control (NT) breast cancer cells versus HSP27 knockdown breast cancer cells (HSP27KD-3), sorted by fold change in the HSP27 knockdown experiment

	Angiogenic vs. nonangiogenic		Control NT vs. HSP27KD-3		
Gene symbol	Fold change	FDR *P* value	Fold change	FDR *P* value	Description
HSPB1	33.4	0.01	6.7	0.01	Heat shock 27 kDa protein
NCF2	1.9	0.07	5.3	0.02	Neutrophil cytosolic factor 2
BST2	7.0	0.01	4.0	0.01	Bone marrow stromal cell antigen 2
SPON2	3.5	0.01	3.1	0.00	Spondin 2, extracellular matrix protein
RAC2	0.7	0.05	3.1	0.03	Ras-related C3 botulinum toxin substrate 2
WARS	1.5	0.06	2.3	0.02	Tryptophanyl-tRNA synthetase
ECGF1	1.2	0.25	2.2	0.02	Endothelial cell growth factor
CXCR4	1.2	0.53	2.2	0.05	Chemokine (C-X-C motif) receptor 4
FN1	0.9	0.51	2.0	0.04	Fibronectin 1
MAPK7	1.0	0.60	1.9	0.05	Mitogen-activated protein kinase 7
IGFBP3	0.7	0.40	1.9	0.07	Insulin-like growth factor binding protein 3
VEGFC	1.0	0.82	1.8	0.05	Vascular endothelial growth factor C
COL18A1	1.1	0.30	1.7	0.04	Collagen, type XVIII, alpha 1
MKNK2	1.0	0.98	1.7	0.03	MAP kinase interacting serine/threonine kinase 2
FGF2	1.1	0.26	1.7	0.05	Fibroblast growth factor 2
CSPG4	1.2	0.26	1.6	0.03	Hondroitin sulfate proteoglycan 4
COL8A2	0.7	0.06	1.6	0.05	Collagen, type VIII, alpha 2
CEACAM1	1.5	0.02	1.6	0.04	Carcinoembryonic antigen-related cell adhesion molecule 1
PTPRB	1.2	0.11	1.6	0.03	Protein tyrosine phosphatase, receptor type, B
DDAH1	1.4	0.13	1.5	0.08	Dimethylarginine dimethylaminohydrolase 1
MMP7	0.6	0.11	1.5	0.02	Matrix metallopeptidase 7
VEGFA	1.0	0.87	1.3	0.02	Vascular endothelial growth factor A
CYR61	0.9	0.23	0.6	0.05	Cysteine-rich, angiogenic inducer, 61
IL11	1.0	0.91	0.5	0.04	Interleukin 11
FGF1	1.1	0.51	0.4	0.03	Fibroblast growth factor 1 (acidic)
TIE-2 (TEK)	0.97	0.53	1.08	0.19	TEK tyrosine kinase, endothelial
PGF	0.84	0.5	0.8	0.28	Placental growth factor

Table S2. GSEA of angiogenesis-related and KEGG pathways in angiogenic control (NT) cells compared with nonangiogenic HSP27KD-3 cells

Gene signature	Enrichment score	Nominal *P* value	FDR *q* value
Angiogenesis-related pathway			
HIF1_TARGETS	−0.66	0	0
MANALO_HYPOXIA	−0.53	0	0.001
HINATA_NFKB	−0.48	0	0.008
VEGF_HUVEC	−0.62	0.039	0.026
STAT3	−0.36	0.059	0.096
STAT3_TF	−0.33	0.054	0.112
KEGG pathway			
HSA04512_ECM_RECEPTOR_INTERACTION	−0.56	0	0.002
HSA04360_AXON_GUIDANCE	−0.48	0	0.029
HSA01430_CELL_COMMUNICATION	−0.47	0.001	0.095
HSA04540_GAP_JUNCTION	−0.47	0.003	0.104
HSA04510_FOCAL_ADHESION	−0.41	0	0.132
HSA04370_VEGF_SIGNALING_PATHWAY	−0.47	0.006	0.136
HSA05219_BLADDER_CANCER	−0.51	0.006	0.125
HSA04670_LEU.K.	−0.43	0	0.129
OCYTE_TRANSENDOTHELIAL_MIGRATION			
HSA00480_GLUTATHIONE_METABOLISM	−0.51	0.019	0.125
HSA04662_B_CELL_RECEPTOR_SIGNALING_PATHWAY	−0.46	0.003	0.139

Differentially regulated pathways were ranked by their corresponding FDR *q* values. Pathway annotations are available at http://www.broad.mit.edu/gsea/msigdb.

Table S3. HSP27 signature: Up-regulated genes in HSP27-expressing cells (NT control) and HSP27 knockdown cells (HSP27KD-3) by high-throughput gene expression analysis (FDR <0.05; fold change >2)

Gene symbol	Fold change	NT, mean ± SD	HSP27KD-3, mean ± SD
HSPB1	6.73	18,294.41 ± 395.00	2,716.53 ± 216.06
NCF2	5.33	2,310.10 ± 88.98	433.75 ± 40.84
RSAD2	4.60	2,248.41 ± 75.05	488.65 ± 42.15
CA9	4.57	2,995.57 ± 216.53	655.01 ± 19.40
ZBTB32	4.41	1,333.32 ± 16.88	302.55 ± 14.17
BST2	4.04	2,371.14 ± 88.16	587.52 ± 81.95
IFIT2	3.91	7,816.07 ± 86.15	2,001.50 ± 264.15
LOC222171	3.70	1,505.95 ± 55.14	407.39 ± 21.32
GDF15	3.68	63,017.85 ± 2,546.54	17,141.76 ± 1,688.92
PTGDS	3.51	3,966.89 ± 188.73	1,130.40 ± 79.68
OASL	3.50	24,098.97 ± 708.82	6,894.95 ± 509.72
OLFML2A	3.44	1,675.78 ± 94.72	487.07 ± 87.28
SLPI	3.41	16,628.13 ± 596.41	4,882.59 ± 515.10
DDIT4	3.26	53,734.53 ± 3,796.42	16,487.81 ± 308.29
ITGB4	3.23	1,732.17 ± 30.03	535.56 ± 54.68
SULF2	3.18	4,629.50 ± 73.07	1,457.48 ± 115.37
SPON2	3.13	23,577.67 ± 379.99	7,539.14 ± 337.78
RAC2	3.10	7,312.19 ± 217.80	2,354.99 ± 76.96
ALOX5	3.10	587.09 ± 19.35	189.28 ± 13.36
LOC389903	3.08	781.00 ± 3.71	253.34 ± 15.87
IFIT3	3.04	1,708.91 ± 45.43	561.76 ± 44.73
IL7R	3.02	2,343.21 ± 115.89	775.53 ± 52.59
LOC340061	3.00	4,683.15 ± 104.46	1,561.18 ± 116.60
IFIT1	2.98	4,339.23 ± 68.58	1,455.73 ± 113.12
CH25H	2.97	3,802.31 ± 253.23	1,280.85 ± 154.18
FGFBP1	2.93	826.09 ± 86.88	282.23 ± 34.78
LOC440731	2.90	1,498.70 ± 69.28	516.09 ± 76.12
RARRES3	2.83	1478.73 ± 85.15	522.26 ± 55.19
RNF185	2.82	1,151.61 ± 103.92	408.63 ± 18.11
IFI44	2.80	11,664.05 ± 191.51	4,172.12 ± 681.16
GBP5	2.70	1,230.16 ± 32.78	455.05 ± 39.97
C19ORF33	2.70	4,422.37 ± 164.28	1,638.50 ± 205.20
C20ORF121	2.64	3,989.55 ± 220.52	1,509.79 ± 28.54
C19ORF32	2.64	1,043.33 ± 35.72	395.00 ± 56.58
LOXL4	2.61	1,755.64 ± 94.50	671.50 ± 47.19
S100A4	2.54	4,109.36 ± 122.41	1,618.89 ± 238.07
H1F0	2.47	4,608.51 ± 244.94	1,864.13 ± 58.77
CSAG1	2.46	684.26 ± 19.22	277.95 ± 37.66
MAL2	2.45	669.71 ± 20.69	273.77 ± 148.02
CCL3	2.44	2,575.79 ± 82.97	1,055.86 ± 35.40
CRLF1	2.40	1,379.69 ± 36.70	575.43 ± 26.20
LOC126755	2.38	344.38 ± 0.82	144.62 ± 43.87
KIAA1522	2.37	21,399.35 ± 1,350.97	9,037.09 ± 480.86
VIPR2	2.35	370.23 ± 44.40	157.21 ± 17.29
KIAA0746	2.34	2,945.90 ± 18.18	1,259.11 ± 23.47
FLJ20035	2.33	989.64 ± 124.54	425.09 ± 36.38
CCL5	2.33	3,158.35 ± 230.86	1,357.72 ± 192.16
PPP1R14C	2.32	841.68 ± 76.16	362.52 ± 12.98
SLC15A4	2.29	2,957.91 ± 146.54	1,289.39 ± 105.79
WARS	2.29	1,0862.41 ± 131.87	4,748.31 ± 295.46
SERPINE2	2.28	6,524.33 ± 287.10	2,862.79 ± 179.93
C2ORF28	2.27	4,225.10 ± 35.79	1,858.03 ± 164.72
PMAIP1	2.26	5,119.90 ± 337.01	2,260.67 ± 373.72
PRKCDBP	2.26	15,773.48 ± 378.86	6,994.75 ± 847.82
PLCG2	2.25	1,550.21 ± 113.49	689.10 ± 41.54
DDIT3	2.25	2,435.88 ± 206.24	1,083.16 ± 37.27
LCN2	2.24	1,200.80 ± 87.28	535.58 ± 14.62
L1CAM	2.22	595.89 ± 29.86	268.78 ± 10.27
FBXO32	2.22	11,755.07 ± 405.85	5,304.69 ± 369.54
LAMA5	2.21	2,182.64 ± 44.94	986.52 ± 247.35
AVPI1	2.21	5,328.09 ± 104.49	2,413.51 ± 103.93

Table S3. Cont.

Gene symbol	Fold change	NT, mean ± SD	HSP27KD-3, mean ± SD
ECGF1	2.21	16,487.99 ± 538.48	7,469.49 ± 632.28
CXCR4	2.20	794.54 ± 18.86	361.13 ± 63.70
S100P	2.20	863.53 ± 53.32	393.32 ± 34.31
SEMA3B	2.20	1,768.78 ± 116.39	805.68 ± 28.28
TNIP2	2.18	3,432.17 ± 98.10	1,573.68 ± 279.38
PI3	2.18	5,229.59 ± 86.11	2,399.59 ± 118.97
C10ORF10	2.18	1,837.25 ± 94.03	843.16 ± 190.40
LOC150371	2.18	1,512.01 ± 84.65	694.86 ± 8.84
CD24	2.16	2,227.87 ± 92.94	1,030.31 ± 94.58
MGC4504	2.16	3,295.41 ± 131.11	1,526.97 ± 40.98
CDR1	2.15	1,435.78 ± 174.05	666.84 ± 87.19
SNTB1	2.14	478.88 ± 5.31	223.28 ± 13.96
XKR8	2.14	24,707.63 ± 641.47	11,562.67 ± 327.90
LRRC54	2.13	1,611.40 ± 72.93	757.73 ± 13.99
GPR30	2.12	1,818.03 ± 120.74	855.67 ± 120.63
NDRG1	2.11	52,299.76 ± 6,966.40	24,779.20 ± 2,962.23
LHPP	2.11	3,671.87 ± 169.84	1,740.11 ± 183.12
KIAA1950	2.09	307.21 ± 15.96	146.64 ± 4.96
GRB10	2.09	7,271.20 ± 173.61	3,472.47 ± 276.63
S100A8	2.08	5,882.44 ± 220.41	2,828.45 ± 364.85
SYTL1	2.08	720.83 ± 18.76	346.80 ± 23.91
CITED2	2.08	3,141.50 ± 37.12	1,512.32 ± 154.68
LOC163782	2.08	667.16 ± 33.35	321.35 ± 6.81
CA12	2.07	11,999.70 ± 449.29	5,800.47 ± 744.45
SLCO3A1	2.07	1,250.38 ± 49.70	605.37 ± 87.35
DDX58	2.06	6,514.22 ± 153.42	3,155.54 ± 208.21
ARF4L	2.06	882.75 ± 71.17	427.66 ± 30.66
DSP	2.06	3,554.07 ± 124.01	1,721.93 ± 208.56
EPS15	2.06	716.32 ± 52.19	347.25 ± 24.77
EPS8L2	2.06	662.89 ± 41.44	321.56 ± 13.22
JDP2	2.06	4,609.15 ± 567.75	2,239.38 ± 66.89
BF	2.05	12,765.07 ± 561.44	6,212.25 ± 773.37
KLF4	2.05	1,687.31 ± 21.66	822.00 ± 106.36
CARD6	2.05	1,047.57 ± 21.77	510.39 ± 27.74
CCL4	2.05	315.92 ± 53.93	154.02 ± 14.94
FN1	2.05	1,906.29 ± 153.33	931.32 ± 241.45
AKR1C1	2.05	5,979.84 ± 261.06	2,923.06 ± 240.24
VANGL1	2.04	3,077.77 ± 122.35	1,508.08 ± 57.99
SFN	2.03	371.52 ± 29.89	182.79 ± 12.72
HES4	2.03	8,833.86 ± 573.53	4,348.58 ± 601.44
SLC35F3	2.02	960.29 ± 32.90	474.26 ± 72.03
PTGS2	2.02	569.77 ± 10.90	281.43 ± 22.04
ISG20	2.02	27,095.09 ± 634.43	13,387.36 ± 218.09
RNUT1	2.02	3,596.73 ± 101.18	1,781.92 ± 61.66
CDC25B	2.02	5,462.82 ± 332.80	2,707.72 ± 256.55
KCNK1	2.02	4,224.51 ± 134.50	2,095.86 ± 99.79
SLC7A11	2.01	1,093.58 ± 130.42	543.04 ± 45.45
SH3TC1	2.01	870.98 ± 23.03	434.02 ± 42.11

Genes are sorted by fold change in the HSP27 knockdown experiment.

Table S4. Multivariate survival analysis of patients with nodular malignant melanoma

Variable	Category	*n*	HR	95% CI	*P* value*
Anatomic site	Other	31	1		
	Trunk	63	5.8	2.8–12.3	<0.001
Level of invasion (Clark)	II, III, IV	73	1		
	V	21	5.6	2.2–13.7	<0.001
Proliferation index (Ki-67)	Low	38	1		
	High	56	1.9	0.89–4.0	0.09
Microvessel density	Low	56	1		
	High	38	2.6	1.3–5.8	0.008
HSP27 expression	Low	34	1		
	High	60	2.2	1.02–4.7	0.044

CI, confidence interval; HR, hazard ratio.
*Likelihood ratio test.